LIMNOLOGY and OCEANOGRAPHY

ASLO

Limnol. Oceanogr. 65, 2020, 387–400

doi: 10.1002/lno.11307

Nature of optical products inverted semianalytically from remote sensing reflectance of stratified waters

Zhongping Lee,[1*] **Shaoling Shang**,[2*] **Yongchao Wang**,[2] **Jianwei Wei**,[1] **Joji Ishizaka**[3]

[1]School for the Environment, University of Massachusetts Boston, Boston, Massachusetts
[2]State Key Lab of Marine Environmental Science, Xiamen University, Xiamen, China
[3]Institute for Space-Earth Environmental Research, Nagoya University, Nagoya, Japan

Abstract

Analytical expressions between inherent optical properties (IOPs) retrieved using semi-analytical algorithms (SAAs) and the vertical distributions of IOPs are derived based on an analytical model for subsurface remote sensing reflectance (r_{rs}). These expressions provide a theoretical and comprehensive understanding of the inverted IOPs for stratified waters and lay the foundation to obtain equivalent products from profiling measurements for apple-to-apple comparison of the remotely sensed properties. It is found that the backscattering coefficient (b_b) derived from an r_{rs} spectrum via an SAA is governed by r_{rs} in the longer wavelengths, consequently the inverted b_b has less (or negligible) contributions from deeper depths, such as the subsurface chlorophyll maximum. In addition, the inverted b_b spectrum does not have the spectral feature of the vertically weighted average b_b. The SAA-derived absorption coefficients, on the other hand, are found related to both the weighting profile at the wavelength of interest and the weighting profile in the longer wavelength(s). As a result, the absorption coefficients in the shorter wavelengths inverted from a perfect SAA are generally lower (can be 40% or more) than its vertically weighted average unless the surface layer dominates the diffuse attenuation of light. Furthermore, unlike the historical perception of remotely sensed chlorophyll concentration (Chl) for stratified waters, SAA-derived Chl is also sensitive to the vertical profile of b_b and tends to be lower than its vertically weighted average assuming perfect bio-optical relationships, unless surface properties dominate the water column.

Concentrations of phytoplankton chlorophyll (Chl, mg m^{-3}) and the inherent optical properties (IOPs) (Preisendorfer 1976) of water can be derived (IOCCG 2000, 2006) from the spectrum of remote sensing reflectance (R_{rs}, sr^{-1}), which is defined as the ratio of water-leaving radiance to downwelling irradiance just above the surface. Through measurements from ocean color satellites, such products are critical for evaluating the spatial-temporal variations of the oceans and large lakes under a changing climate (Gregg and Conkright 2002; Boyce et al. 2014; Signorini et al. 2015). Based on a large number of field measurements, the production of Chl from R_{rs} generally takes an empirical band-ratio approach (Gordon and Morel 1983; O'Reilly et al. 1998), a tradition that is still followed today, which can be expressed as

$$\mathrm{Chl}^{\mathrm{RS}} = 10^{\alpha_0 + \alpha_1 \times \mathrm{RR} + \alpha_2 \times \mathrm{RR}^2 + \alpha_3 \times \mathrm{RR}^3 + \alpha_4 \times \mathrm{RR}^4}, \quad (1a)$$

$$\mathrm{RR} = \log_{10}\left(\frac{\mathrm{Max}(R_{rs}(\lambda_1), R_{rs}(\lambda_2), R_{rs}(\lambda_3))}{R_{rs}(\lambda_4)}\right). \quad (1b)$$

Here, λ_{1-3} are wavelengths in the range of ~ 440–510 nm, with λ_4 around 550 nm. Superscript "RS" represents a property derived from ocean color remote sensing. α_{0-4} are empirical coefficients derived by fitting Eq. 1 for a data set containing a wide range of Chl and RR.

For vertically homogeneous waters, $\mathrm{Chl}^{\mathrm{RS}}$ can be compared with Chl measured at any depth in the upper layer to evaluate the accuracy of $\mathrm{Chl}^{\mathrm{RS}}$ or the performance of an inversion algorithm. Due to interactions of light and nutrient distributions as well as dynamic processes, however, the vertical distribution of Chl or suspended sediment can be stratified (Morel and Berthon 1989; Churnside and Donaghay 2009; Cullen 2015; Moore et al. 2019). Various studies (e.g., Sathyendranath and Platt 1989; Zaneveld et al. 1998; Forget et al. 2001; Kutser et al. 2008) have demonstrated that such vertical variations of Chl or suspended sediment can have serious influence on R_{rs} or irradiance reflectance. To help the interpretation of $\mathrm{Chl}^{\mathrm{RS}}$ of such stratified waters, Gordon and Clark (1980) and Gordon (1992) proposed that $\mathrm{Chl}^{\mathrm{RS}}$ can be considered as a

*Correspondence: zhongping.lee@umb.edu (Z. L.) or slshang@xmu.edu.cn (S.S.)

Additional Supporting Information may be found in the online version of this article.

weighted average of the vertical profile of chlorophyll concentration (Chl(z)), expressed as

$$\langle \mathrm{Chl}(\lambda)\rangle_{\mathrm{GC}} = \int_0^\infty \mathrm{Chl}(z) w_{\mathrm{GC}}(z,\lambda) dz. \quad (2)$$

Here, symbol "<>$_{GC}$" represents a vertically weighted average of a property following Gordon and Clark (1980), and $w_{GC}(z,\lambda)$ is the weighting profile at wavelength λ (nm) proposed by Gordon and Clark (1980) and Gordon (1992),

$$w_{\mathrm{GC}}(z,\lambda) = \frac{\exp(-2\tau(z,\lambda))}{\int_0^\infty \exp(-2\tau(z,\lambda))dz}, \quad (3a)$$

with

$$2\tau(z,\lambda) = \int_0^z (K_{\mathrm{d}}(z',\lambda) + \kappa_u(z',\lambda))\, dz' \quad (3b)$$

and

$$\int_0^\infty w_{\mathrm{GC}}(z,\lambda) dz = 1. \quad (3c)$$

Here, z (in m) is water depth from surface and positive downward, "2τ" simply indicates the round-trip attenuation of diffused light from surface-to-depth and back-to-surface. $K_{\mathrm{d}}(z, \lambda)$ (in m^{-1}) is the diffuse attenuation coefficient of downwelling irradiance at wavelength λ, while $\kappa_u(z, \lambda)$ (in m^{-1}) is the diffuse attenuation coefficient for radiance backscattered at depth z propagating toward the surface (Philpot 1987). Gordon and Clark (1980) and Gordon (1992) indicted that a use of K_{d} to replace κ_u resulted in negligible impact on <Chl(λ)>$_{GC}$, a practice also followed here. Note that $2\tau(\lambda)$ and <Chl(λ)>$_{GC}$ are spectrally dependent, while Chl^{RS} of Eq. 1 is associated with at least two wavelengths. Sathyendranath and Platt (1989) therefore suggested to use the smaller $2\tau(\lambda)$ among the two wavelengths for the weighting calculation, as the light at this wavelength penetrates deeper to encounter the layer of maximum Chl; while Morel and Berthon (1989) used K_{PAR} (the diffuse attenuation coefficient of the photosynthetic available radiation) to represent the average of ($K_{\mathrm{d}} + \kappa_u$). The integration to ∞ in Eqs. 2, 3 can be truncated to the penetration depth (D, in m) (Gordon and Mcluney 1975), as the contributions from D to ∞ are small (< 10%) due to the two-way exponential attenuation of light.

The above system for evaluation of Chl^{RS} of stratified waters has been adopted by the community in the past decades to evaluate various retrievals (Smith 1981; Gordon et al. 1983; Lee et al. 2013; Werdell et al. 2014). In the recent decades, however, an important advance in ocean color algorithms is the development and application of analytical or semianalytical algorithms (SAAs) for both Chl and the IOPs (in particular the absorption and backscattering coefficients) (Lee et al. 2002; IOCCG 2006; Werdell et al. 2013*b*). Although we now have a solid understanding on how stratified waters impact R_{rs} at each wavelength (Sathyendranath and Platt 1989; Gordon 1992; Zaneveld et al. 2005), it is very different when inverting R_{rs} of stratified waters for IOPs or Chl with an SAA. This is because, unlike the band-ratio algorithm for Chl, an SAA, in particular the spectral optimization algorithms (SOAs) (Roesler and Perry 1995; Lee et al. 1999; Maritorena et al. 2002; Huang et al. 2013; Werdell et al. 2018), uses all or most available R_{rs} values to simultaneously retrieve a set of bio-optical properties. Since the impact of stratification on R_{rs} is wavelength-dependent (Sathyendranath and Platt 1989; Gordon 1992; Zaneveld et al. 2005), it is actually unknown how such a spectral variation of stratification influences the SAA retrievals; or if the obtained Chl^{RS} or IOPs^{RS} from an SAA can still be evaluated using the classic weighted average (Gordon and Clark 1980; Gordon 1992) as shown in Eq. 2. For instance, Werdell et al. (2014) showed that the inverted concentrations of *Noctiluca miliaris* and diatoms biased lower than the weighted averages for stratified cases, which is attributed to imperfection of the optimization algorithm. However, could the method of weighted averaging also contribute to this discrepancy? Ideally, to avoid this dilemma, it is required to obtain the vertical distributions of water constituents from ocean color reflectance, but this can only be limited to situations where all profile related parameters can be described using one variable (Morel and Berthon 1989), or the vertical profiles are known a priori (Xue et al. 2015). This is because fundamentally there are multiple variables to determine an R_{rs} spectrum, which make the analytical inversion of R_{rs} an "ill-posed" mathematical problem (Defoin-Platel and Chami 2007), unless the focus is simply the backscattering coefficient in the longer wavelengths (Lee et al. 2002).

To fill the gap in understanding SAA-derived Chl^{RS} or IOPs^{RS} of stratified waters, we here present theoretical expressions of the analytically inverted IOPs for stratified waters, which show that SAA-inverted IOPs^{RS} are far more complex than the classic model (Gordon and Clark 1980; Gordon 1992), and the absorption and backscattering coefficients are associated with different ways of "weighted averaging." The results here will not only provide a comprehensive understanding of IOPs and Chl inverted from R_{rs} of stratified waters, but also reduce uncertainties when comparing remotely sensed products with measurements for such waters.

Brief review of SAAs for IOPs

Unlike simple band-ratio type empirical algorithms for water properties (e.g., Chl, or absorption coefficients), an SAA employs a relationship between R_{rs} and IOPs and uses R_{rs} measurements from ~ 400 nm to ~ 700 nm (or even longer wavelength) to carry out the derivation (Doerffer and Fisher 1994; Maritorena et al. 2002; Werdell et al. 2013*a*). Without loss of generality, the following uses the quasi-analytical algorithm

(QAA) (Lee et al. 2002) as an example to describe this kind of inversion algorithms.

An SAA like QAA employs a model for subsurface remote sensing reflectance (r_{rs}) for the inversion, where r_{rs} can be accurately calculated from R_{rs} (Gordon et al. 1988; Lee et al. 2002). The model for r_{rs} usually takes the following form (Gordon et al. 1988):

$$r_{rs} = (g_0 + g_1 u)u. \tag{4}$$

Here, g_0 and g_1 are model constants, u, which can be derived algebraically from known r_{rs}, is a function of the inverted IOPs,

$$u(\lambda) = \frac{b_b^{RS}(\lambda)}{a^{RS}(\lambda) + b_b^{RS}(\lambda)}, \tag{5}$$

with b_b^{RS} and a^{RS}, respectively, the products of backscattering and absorption coefficients to be derived from an SAA. There are other forms developed to model r_{rs} as a function of IOPs (e.g., Lee et al. 2004; Park and Ruddick 2005; Twardowski and Tonizzo 2018), but the overall nature is the same as that expressed by Eq. 4, although some model coefficients and expressions are different.

Because there are two unknowns (a and b_b) for r_{rs} at each wavelength, QAA starts the estimation of absorption at the longer (or reference) wavelength (λ_0), expressed as

$$a^{RS}(\lambda_0) = a_w(\lambda_0) + \Delta a(\lambda_0) = a_w(\lambda_0) + f(r_{rs}). \tag{6}$$

This is because $a_w(\lambda_0)$ dominates $a(\lambda_0)$ in the longer wavelengths, thus $r_{rs}(\lambda_0)$ can be approximated as just a function of variable $b_b(\lambda_0)$, and the math problem is less or no longer "ill-posed." $f(r_{rs})$ here is an empirical function for the estimation of $a^{RS}(\lambda_0)$, and this is a key step in QAA as it initiates the calculations and plays an important role in determining the accuracy of the inverted IOPs (Lee et al. 2010).

After $a^{RS}(\lambda_0)$ is known, $b_b^{RS}(\lambda_0)$ can be calculated algebraically from Eq. 5,

$$b_b^{RS}(\lambda_0) = \frac{u(\lambda_0)a^{RS}(\lambda_0)}{1 - u(\lambda_0)}. \tag{7}$$

Furthermore, the backscattering coefficient of particles (b_{bp}) is calculated by subtracting off the backscattering coefficient of pure seawater (b_{bw}) from b_b. $b_b^{RS}(\lambda_0)$ is then extended to the other wavelengths following

$$b_b^{RS}(\lambda) = b_{bw}(\lambda) + b_{bp}^{RS}(\lambda_0)\left(\frac{\lambda_0}{\lambda}\right)^Y. \tag{8}$$

Here, parameter Y is estimated empirically from the measured R_{rs} spectrum (Lee et al. 2002). After $b_b^{RS}(\lambda)$ is known, $a^{RS}(\lambda)$ can be calculated algebraically from Eq. 5,

$$a^{RS}(\lambda) = \frac{b_b^{RS}(\lambda)(1 - u(\lambda))}{u(\lambda)}. \tag{9}$$

After the total absorption coefficients are derived from r_{rs}, they can further be decomposed into contributions of phytoplankton pigments and colored dissolved organic matter (Lee et al. 2002; Dong et al. 2013; Zheng et al. 2015; Grunert et al. 2019). Results from QAA have been shown to be very successful for the derivation of IOPs (IOCCG 2006; Chen and Zhang 2015; Gomes et al. 2018), as it employs limited empirical relationships at least for the derivation of the total absorption and backscattering coefficients (Lee et al. 2002). The above processes and products assume the water column is homogeneous, where the nature of the retrieved $b_b^{RS}(\lambda)$ and $a^{RS}(\lambda)$ becomes unknown if the water is stratified. In other words, if the water is stratified and there are measurements of IOP profiles, it is not clear if the above derived $b_b^{RS}(\lambda)$ and $a^{RS}(\lambda)$ should be compared with their weighted averages following Eq. 2, although some studies (Lee et al. 2013; Werdell et al. 2014) took this approach without rigorous scrutiny.

Model of r_{rs} for stratified waters

For stratified waters, based on numerical simulations, Gordon (1992) suggested that r_{rs} can still be modeled by Eq. 4, but u should be replaced by $\langle u \rangle_{GC}$, which is a weighted average similarly like $\langle Chl \rangle_{GC}$,

$$\langle u \rangle_{GC} = \int_0^\infty u(z) w_{GC}(z) dz, \tag{10}$$

with $u(z)$ the depth profile of the ratio of $b_b(z)$ to $a(z) + b_b(z)$,

$$u(z) = \frac{b_b(z)}{a(z) + b_b(z)}. \tag{11}$$

Note that wavelength is omitted for brevity, unless it is required for clarification.

However, based on a two-stream model derived from the radiative transfer equation (Aas 1987), Zaneveld et al. (2005) showed that the weighted average of $u(z)$ for r_{rs} of stratified waters follows a different weighting and results in a different weighted-average (represented as $\langle u \rangle_Z$). This average can be expressed as

$$\langle u \rangle_Z = \int_0^\infty u(z) w_Z(z) dz, \tag{12}$$

with the weighting factor $w_Z(z)$ as (Zaneveld et al. 2005),

$$w_Z(z) = \left[\frac{d}{dz}\exp\left(-\int_0^z (K_d(z') + \kappa_u(z'))dz'\right)\right], \tag{13a}$$

which can be written as

$$w_Z(z) = \exp(-2\tau(z))(K_d(z) + \kappa_u(z)), \quad (13b)$$

and,

$$\int_0^\infty w_Z(z)dz = 1. \quad (13c)$$

We here use "$<>_Z$" to represent a weighted average of a property following Zaneveld et al. (2005). Note that in the above expressions g_0 and g_1 for the r_{rs} model (Eq. 4) are assumed constant vertically.

Comparing Eq. 13b with Eq. 3a, it shows large differences in the weighting of different layers contributing to R_{rs} (or r_{rs}), where the weighting is proportional to round trip attenuation with the Gordon and Clark (1980) model, but proportional to the derivative of round trip attenuation with the Zaneveld et al. (2005) model. In other words, Eq. 13b indicates that u for subsurface remote sensing reflectance of stratified waters is not an average of $u(z)$ weighted by two-way attenuation of light, rather with a two-way attenuation modulated by the diffuse attenuation coefficient (Zaneveld et al. 2005). Such a weighting mechanism is also consistent with the derivations based on the single scattering approximation (Philpot 1987). This difference in weighting factor is further demonstrated in Fig. 1 for a synthesized Chl profile (Fig. 1a), with values of K_d calculated from Hydrolight (HL) simulations (Mobley and Sundman 2013), where simulation of the IOP profiles is described in Supporting Information Appendix. For this case where surface Chl is 0.2 mg m^{-3}, weightings (or contributions) of the near surface layers to r_{rs} are just about 1%, and it is the top ~ 18.5 m that contributes 90% of r_{rs} at 440 nm based on Eq. 13, but ~ 14.5 m for 550 nm. In other words, light at 440 nm "feels" much more of this chlorophyll maximum layer than light at 550 nm for this case. In addition, the contributions to r_{rs} from the layer of maximum Chl (at 20 m) are found enhanced with the Zaneveld et al. (2005) model, with $w_Z(20,440)$ nearly a factor of 2 of $w_{GC}(20,440)$ for this case. In the following, although weighting profiles described by Eqs. 3a, 13b are the same if τ is independent of depth, the model of Zaneveld et al. (2005) for r_{rs} is adopted for the derivations of retrieved IOPs for stratified waters.

General relationships for QAA-inverted IOPs of stratified waters

Absorption coefficient at the reference wavelength

In QAA (v6) (http://www.ioccg.org/groups/software.html), $a^{RS}(\lambda_0)$ is estimated empirically as

$$a^{RS}(\lambda_0) = a_w(\lambda_0) + f\left(\frac{r_{rs}(440), r_{rs}(490)}{r_{rs}(550), r_{rs}(670)}\right), \quad (14)$$

Since r_{rs} is a function of u (*see* Eq. 4), Eq. 14 effectively is

$$a^{RS}(\lambda_0) = a_w(\lambda_0) + f\left(\frac{\int_0^\infty u(z,440)w_Z(z,440)dz,\ \int_0^\infty u(z,490)w_Z(z,490)dz}{\int_0^\infty u(z,550)w_Z(z,550)dz,\ \int_0^\infty u(z,670)w_Z(z,670)dz}\right). \quad (15)$$

This expression shows the complex nature of $a^{RS}(\lambda_0)$ when the water is stratified, especially due to the association of different wavelengths where the weighting factors differ spectrally. On the other hand, because of the empirical nature of this estimation, the $a^{RS}(\lambda_0)$ of Eq. 14 depends on the choice of absorption property used for the development of the empirical relationship. Following Eq. 12, it makes more sense, and is consistent to radiative transfer, to use $<a>_Z$ at λ_0 for this property. Thus, for stratified waters, the targeted $a^{RS}(\lambda_0)$ of QAA is

$$a^{RS}(\lambda_0) = \int_0^\infty a(z,\lambda_0)w_Z(z,\lambda_0)dz, \quad (16a)$$

or,

$$a^{RS}(\lambda_0) = a_w(\lambda_0) + \langle a_{nw}(\lambda_0)\rangle_Z. \quad (16b)$$

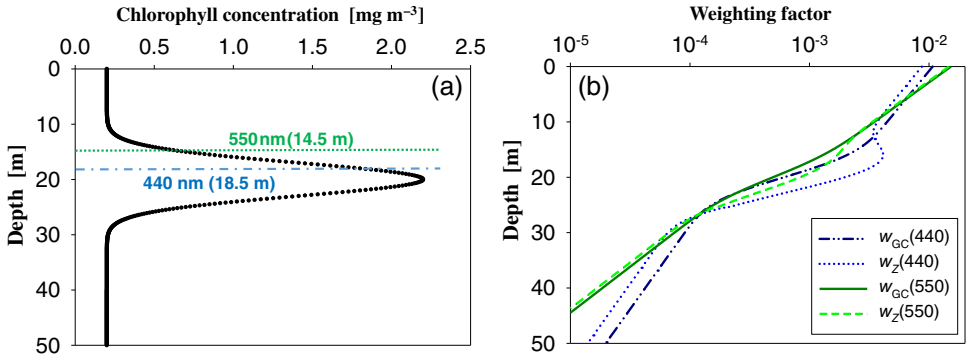

Fig. 1. (**b**) Profiles of weighting factors at 440 and 550 nm for a synthesized stratified Chl profile (**a**), with weighting factors following the models of Gordon and Clark (1980) and Zaneveld et al. (2005), respectively. The blue green lines in (**a**) indicate the penetration depths of 440 nm and 550 nm, respectively. Corresponding profiles of IOPs are described in Supporting Information Appendix.

Here, a_{nw} represents contributions to the total absorption coefficient from nonwater components. In short, to cover both homogeneous and stratified waters, the algorithm coefficients of Eq. 14 should be tuned using absorption data calculated through Eq. 16. However, because λ_0 is generally in the green to red/infrared spectral domain, due to higher $\tau(\lambda_0)$ from the higher $a_w(\lambda_0)$ values, $a^{RS}(\lambda_0)$ represents primarily properties near the surface, where contributions from a layer of subsurface constituents, such as the layer of maximum chlorophyll, will be limited unless this layer is near or on the surface (*see* Fig. 1 for example).

As examples, Fig. 2 shows change of $a^{RS}(550)$ derived from QAA, along with changes of $<a(550)>_Z$, for four synthesized cases with different depths of chlorophyll maximum, where, as expected, the impact to $a^{RS}(550)$ from deep Chl maximum for these simulations appears small (< 9% between z_{max} = 10 m and z_{max} = 40 m). Therefore, in the following, all derivations and discussions are based on this observation or assumption that $a^{RS}(\lambda_0)$ approximates $<a(\lambda_0)>_Z$, which is also because that in general we can select (or employ) longer λ_0 for the estimation of $a^{RS}(\lambda_0)$.

Backscattering coefficient at the reference wavelength

In QAA, u is inverted through Eq. 4. Following Eq. 12, there is

$$\frac{b_b^{RS}}{a^{RS}+b_b^{RS}} = \langle u \rangle_Z. \tag{17}$$

Because QAA starts from λ_0, where generally $a >> b_b$ at such longer wavelengths, the above equation approximates,

$$\frac{b_b^{RS}(\lambda_0)}{a^{RS}(\lambda_0)} \approx \int_0^\infty \frac{b_b(z,\lambda_0)}{a(z,\lambda_0)} w_Z(z,\lambda_0) dz. \tag{18}$$

Applying Eq. 16b, there is

$$b_b^{RS}(\lambda_0) \approx \int_0^\infty \frac{a_w(\lambda_0)+\langle a_{nw}(\lambda_0)\rangle}{a_w(\lambda_0)+a_{nw}(z,\lambda_0)} b_b(z,\lambda_0) w_Z(z,\lambda_0) dz. \tag{19}$$

Thus, for cases where $a_w(\lambda_0) >> a_{nw}(\lambda_0)$, such as oceanic waters and λ_0 = 550 nm or longer wavelengths for coastal waters (Lee et al. 2002), the above becomes

$$b_b^{RS}(\lambda_0) \approx \int_0^\infty b_b(z,\lambda_0) w_Z(z,\lambda_0) dz. \tag{20a}$$

or

$$b_b^{RS}(\lambda_0) \approx \int_0^\infty b_b(z,\lambda_0) \exp(-\tau(z,\lambda_0)) (K_d(z,\lambda_0)+\kappa_u(z,\lambda_0)) dz. \tag{20b}$$

This expression, which shows the associated weighting parameters, is key for understanding $b_b^{RS}(\lambda_0)$ retrieved by QAA or other SAAs of stratified waters, that is, the retrieved $b_b^{RS}(\lambda_0)$ (and then $b_{bp}^{RS}(\lambda_0)$) can be considered as a weighted average of the vertical $b_b(z, \lambda_0)$. This is consistent with Zaneveld et al. (2005) for the case when absorption coefficient is nearly a constant vertically.

Backscattering coefficient at other wavelengths

The backscattering coefficient at other wavelengths in QAA is extended from $b_b^{RS}(\lambda_0)$ via Eq. 8,

$$b_b^{RS}(\lambda) = b_{bw}(\lambda) + \left[\int_0^\infty b_{bp}(z,\lambda_0) w_Z(z,\lambda_0) dz\right] \left(\frac{\lambda_0}{\lambda}\right)^Y. \tag{21}$$

This equation indicates that $b_b^{RS}(\lambda)$ of stratified waters derived via QAA is generally weighted by attenuation in the longer wavelength (λ_0), instead of the weighting factor at the wavelength of interest. This is very different from the weighting scheme (Eq. 2) proposed by Gordon and Clark

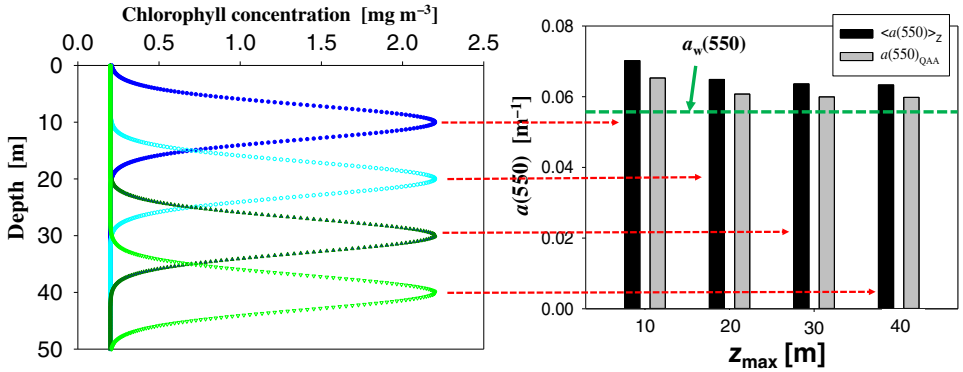

Fig. 2. Impact of z_{max} on the values of $<a(550)>_Z$ and $a(550)_{QAA}$. (Left) Four Chl profiles, with change only in z_{max} (10, 20, 30, and 40 m); (right) corresponding values of $<a(550)>_Z$ and $a(550)_{QAA}$ for the four Chl profiles.

(1980). As an example, Fig. 3b compares $b_{bp}^{RS}(\lambda)$ with $<b_{bp}(\lambda)>_Z$ for a stratified case with a layer of maximum chlorophyll at 20 m (Fig. 3a), where $b_{bp}^{RS}(\lambda)$ is ~ 30% smaller than $<b_{bp}(\lambda)>_Z$ for wavelengths in the ~ 400–500 nm range for this case. In particular, because Y value is given (either estimated or fixed), $b_{bp}^{RS}(\lambda)$ is a smooth power-law function of wavelength and does not have the spectral variation presented in $<b_{bp}(\lambda)>_Z$, a spectral feature contributed by the spectrally varying $w_Z(\lambda)$. In order words, because $b_{bp}^{RS}(\lambda)$ is extended from $b_{bp}^{RS}(\lambda_0)$ in QAA (or SAA), the weighting factor for $b_{bp}^{RS}(\lambda)$ obtained in QAA (or SAA) is not $w_Z(\lambda)$, rather $w_Z(\lambda_0)$. Therefore, when comparing QAA-derived b_b^{RS} (or b_{bp}^{RS}) with in situ measurements for stratified waters, the $b_b(z)$ (or $b_{bp}(z)$) from measurements should not be weight-averaged via Eq. 12 for b_{bp} of interested wavelength, rather weight-averaged using weighting factors in the longer wavelength.

Separately, due to the high $a_w(\lambda_0)$ values, b_b^{RS} (then b_{bp}^{RS}) has limited or no contributions from deeper layers, such as the layer of Chl maximum commonly observed in the open ocean. On the other hand, for λ longer than λ_0, if $b_{bp}^{RS}(\lambda_0)$ has some information of subsurface Chl maximum, $b_{bp}^{RS}(\lambda)$ will tend to be larger than $<b_{bp}(\lambda)>$. This is because $b_{bp}^{RS}(\lambda)$ is extended from $b_{bp}^{RS}(\lambda_0)$ (Eq. 21), and $<b_{bp}(\lambda)>$ has less vertical information than $<b_{bp}(\lambda_0)>$ for the longer λ due to larger $\tau(\lambda)$ values.

Absorption coefficient at the shorter wavelengths

Applying the above derived $b_b^{RS}(\lambda)$ to Eq. 17, we have

$$a^{RS}(\lambda) = b_b^{RS}(\lambda)\frac{1-\langle u(\lambda)\rangle_Z}{\langle u(\lambda)\rangle_Z}. \quad (22)$$

Considering generally $a >> b_b$, Eq. 22 could be approximated as

$$a^{RS}(\lambda) \approx b_b^{RS}(\lambda)\frac{1}{\int_0^\infty \left(\frac{b_b(z,\lambda)}{a(z,\lambda)}\right) w_Z(z,\lambda)dz}. \quad (23a)$$

Or, to spell out the weighting factor associated with $b_b^{RS}(\lambda)$, it is

$$a^{RS}(\lambda) \approx \left\{ b_{bw}(\lambda) + \left[\int_0^\infty b_{bp}(z,\lambda_0) w_Z(z,\lambda_0)dz\right]\left(\frac{\lambda_0}{\lambda}\right)^Y \right\} \frac{1}{\int_0^\infty \left(\frac{b_b(z,\lambda)}{a(z,\lambda)}\right) w_Z(z,\lambda)dz}. \quad (23b)$$

This expression shows a very different, and complex, relationship for QAA derived absorption coefficient compared to the classic weighted average (Eq. 2) when water is stratified. Specifically,

1. $a^{RS}(\lambda)$ of stratified waters is not only determined by the weighting factors at λ, but also by the weighting factor at λ_0, or the longer wavelengths in general.
2. $a^{RS}(\lambda)$ is not simply the weighted average of $a(z, \lambda)$, rather it is governed by the vertical profiles of both b_b and u. This result shows that the classical vertically weighted average showing by Eq. 2 is not applicable to SAA-derived absorption coefficients, where Eq. 2 shows that the weighted average has no association of multiple IOPs except the round-trip attenuation of light at the interested wavelength. Equation 23 rather suggests that for stratified waters, it requires detailed profile measurements of at least $b_b(z)$ and $a(z)$ when a^{RS} is compared with in situ measurements.
3. In addition, because mathematically the average of $1/a$ emphasizes smaller a values, while the average of a emphasizes larger a values, Eq. 23 indicates in general $a^{RS}(\lambda)$ will be lower than $<a(\lambda)>_Z$ for stratified waters. Fundamentally, this is due to that, although weighted by $w_Z(z)$, $<b_b/a>$ (or r_{rs}) is driven by larger values of $b_b(z)/a(z)$, not larger values of $a(z)$.

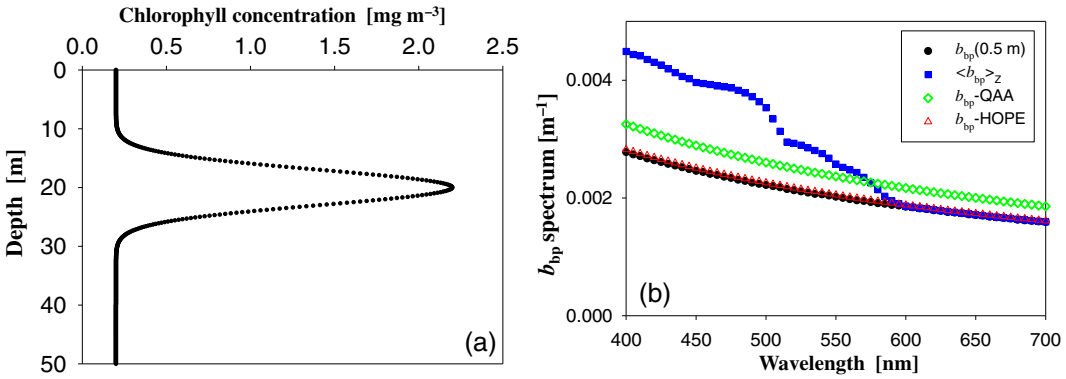

Fig. 3. (b) Spectra of b_{bp} at 0.5 m, weight-averaged following Zaneveld et al. (2005), and that obtained from QAA and HOPE (*see* "Implication for spectral optimization algorithms" section regarding HOPE), respectively, for a synthesized Chl profile (a, z_{max} = 20 m). In the inversion process, to focus on the impact of stratification, Y value was set as 1.0 to match its known value. See Supporting Information Appendix for corresponding IOPs profiles for this Chl profile.

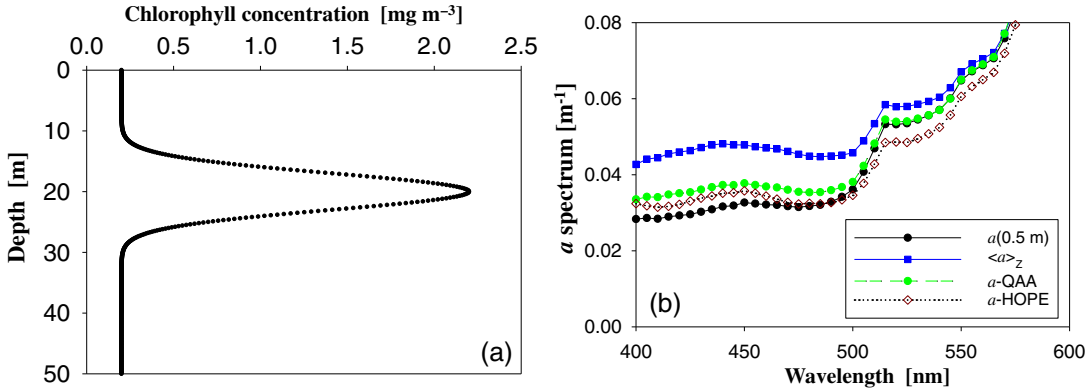

Fig. 4. (b) Spectra of a at 0.5 m, weight-averaged following Zaneveld et al. (2005), and that obtained from QAA and HOPE, respectively, for a synthesized Chl profile (a, z_{max} = 20 m). See Supporting Information Appendix for corresponding IOPs profiles for this Chl profile.

4. Furthermore, because $b_b^{RS}(\lambda)$ is in general smaller than $<b_b(\lambda)>_Z$, this feature further enhances the overall tendency of lower $a^{RS}(\lambda)$ compared to $<a(\lambda)>_Z$, unless the surface layer dominates the diffuse attenuation of light.
   As an example, Fig. 4b compares $a^{RS}(\lambda)$ from QAA vs. $<a(\lambda)>_Z$ for the Chl profile of Fig. 4a, where $a^{RS}(\lambda)$ from QAA is smaller by ~ 40% compared to $<a(\lambda)>_Z$ for wavelengths ~ 400–500 nm.
   Note that in the above example, it is $<a(\lambda_0)>_Z$ used for the derivation of $b_b^{RS}(\lambda_0)$. If it is the $a(\lambda_0)$ value just below the surface (black line in Fig. 4b) used, even smaller $b_b^{RS}(\lambda_0)$ (then $a^{RS}(\lambda)$) will result because $a(\lambda_0)$ just below the surface is smaller than $<a(\lambda_0)>_Z$ for such a case.

If the water is stratified in a way that the layer of maximum constituents is on the sea surface, the retrieved $b_b^{RS}(\lambda)$ and $a^{RS}(\lambda)$ will match better with $<b_b(\lambda)>_Z$ and $<a(\lambda)>_Z$, respectively, due to both higher $b_b(\lambda)$ and $a(\lambda)$ values from this layer and the significantly greater weightings from the near surface. Certainly the closeness in agreement is dependent on the details of such stratifications.

Discussion

Implication for SOAs

Are the above conclusions for QAA applicable for an SOA when applied to stratified waters? To answer this, let us briefly review the steps of an SOA. The goal and outcomes of SOAs are simultaneously, and numerically, to solve Eqs. 4 or 5 for a few (usually three) variables by minimizing the difference between measured and modeled r_{rs} (or u) spectra. During this process, the total absorption and backscattering coefficients are generally modeled as (Lee et al. 1999; Maritorena et al. 2002)

$$a^{RS}(\lambda) = a_w(\lambda) + M_1 * a_{ph}^*(\lambda) + M_2 * a_{dg}^*(\lambda). \quad (24a)$$

$$b_b^{RS}(\lambda) = b_{bw}(\lambda) + M_3 * b_{bp}^*(\lambda). \quad (24b)$$

Here, M_{1-3} are magnitude variables that are desired and to be derived from an r_{rs} spectrum, while $a_{ph}^*(\lambda)$, $a_{dg}^*(\lambda)$, and $b_{bp}^*(\lambda)$ are spectral shapes determined from bio-optical models. The above a^{RS} and b_b^{RS} spectra are applied to Eq. 5 to get modeled u and r_{rs} spectra, and values of M_{1-3} are derived numerically by minimizing the difference ($\delta_{R_{rs}}$, *see* Eq. 25) between the modeled r_{rs} (or u) spectrum and the measured r_{rs} (or u) spectrum for wavelengths in the blue-red (or blue-infrared for very turbid waters).

$$\delta_{R_{rs}} = \frac{\sqrt{\Lambda\left(\left(R_{rs}^{mea}(\lambda_i) - R_{rs}^{mod}(\lambda_i)\right)^2\right)}}{\Lambda\left(R_{rs}^{mea}(\lambda_i)\right)}. \quad (25)$$

Here, Λ represents average of a property for wavelengths employed in the optimization process.

Unlike QAA where the inversion processes and steps are explicit, processes of an SOA inversion are implicit, so it is not obvious on how M_{1-3} are derived. However, the explanation of QAA results is portable to the results of an SOA. Partially it is because results of QAA and an SOA are nearly identical at least for homogeneous waters (Lee et al. 2002), also because the physics of an SOA is the same as QAA. Specifically,

1. Although it is the entire r_{rs} (R_{rs}) spectrum (multiband or hyperspectral) used for the inversion of M_{1-3}, it is primarily r_{rs} (or u) in the longer wavelengths determining the value of M_3. This is due to that only in the longer wavelengths (approximately > 550 nm or wavelengths in the red/-infrared for more productive waters) values of a_w are significantly greater than the contributions from a_{ph} and a_{dg} as well as that from b_{bp}, u^{mod} can be approximated as

$$u^{mod}(\lambda) \approx \frac{M_3 * b_{bp}^*(\lambda)}{a_w(\lambda)}. \quad (26)$$

Therefore, the value of M_3 (or b_{bp}) can be derived, numerically, by comparing u^{mod} with u^{RS}. So, as articulated for QAA derived b_{bp}, because it is the r_{rs} (u) data in the longer wavelengths used for the derivation of b_{bp}, this property from an SOA may not have the contribution from deeper depths. Also, because it is the same type of b_{bp}^* spectral shape (Eq. 8) used to obtain the b_{bp} spectrum in an SOA (Maritorena et al. 2002; Werdell et al. 2013*a*), the resulted b_{bp} spectrum will not have the spectral feature of $<b_{bp}(\lambda)>_Z$. Furthermore, the resulted absorption coefficient will also tend to be lower than $<a(\lambda)>_Z$ assuming a perfect SOA at least for homogeneous waters, unless it is a stratified water column where the surface layer dominates the diffuse attenuation of light.

To demonstrate these features, the hyperspectral optimization process exemplar (HOPE) described in Lee et al. (1999) was applied to the r_{rs} spectrum (400–700 nm, 5 nm step) of the Chl profile showing in Fig. 3a. The resulted $b_{bp}^{RS}(\lambda)$ and $a^{RS}(\lambda)$ spectra are included in Figs. 3b, 4b, respectively. As articulated above, although there is a strong chlorophyll maximum at 20 m, the $b_{bp}^{RS}(\lambda)$ from HOPE are lower (by ~ 40%) than $<b_{bp}(\lambda)>_Z$ for wavelengths of 400–550 nm range, and lower (by ~ 10%) than that from QAA. This lower HOPE-$b_{bp}^{RS}(\lambda)$ is due to the use of r_{rs} in the even longer wavelengths (600–700 nm) in the inversion process, where the contribution of b_{bp} from deeper depths to r_{rs} is negligible, thus the inverted $b_{bp}^{RS}(\lambda)$ is primarily determined by subsurface values, as show in Fig. 3b (see the red vs. black spectra). Furthermore, due to the lower $b_{bp}^{RS}(\lambda)$, the resulted $a(\lambda)^{RS}$ from HOPE is also lower (by ~ 10%) than that from QAA for the ~ 400–550 nm range. In addition, HOPE-$a^{RS}(\lambda)$ spectrum shows different spectral shapes from QAA-$a^{RS}(\lambda)$ spectrum. This is because HOPE-a^{RS} is a sum of the component absorption coefficient where errors in $a_{ph}^*(\lambda)$ and $a_{dg}^*(\lambda)$ will propagate to $a^{RS}(\lambda)$ (and $\delta_{R_{rs}}$), while QAA-$a^{RS}(\lambda)$ is an inversion of r_{rs} without assumptions in $a_{ph}^*(\lambda)$ and $a_{dg}^*(\lambda)$. Note that these findings are also applicable to the Garver–Siegel–Maritorena (GSM) algorithm (Maritorena et al. 2002) or the generalized IOP algorithm (GIOP) (Werdell et al. 2013*a*), as the overall algorithm structures of those SOAs are the same as that of HOPE, except the bio-optical models for component IOPs and the computation architecture.

2. Because Chl^{RS} is primarily derived from $a^{RS}(\lambda)$ through SAAs, Chl^{RS} will also be a complex average involving profiles of Chl and IOPs as indicated by Eq. 23, not as the classic relationship described by Eq. 2. Furthermore, because $a^{RS}(\lambda)$ in the shorter wavelengths will be lower in general than the weighted average for a stratified water, SAAs-inverted Chl^{RS} will also tend to be lower compared to the weighted average even assuming perfect relationships between the absorption coefficient and Chl. This inherent spectrally varying effect of stratified water in an SAA provides a sound explanation for the underestimated concentrations of *N. miliaris* and diatoms compared to the vertically weighted values (Werdell et al. 2014), where the GIOP was implemented to invert vertically stratified distributions of *N. miliaris* and diatoms. In other words, the agreement between the R_{rs} inversion and the known values will be better if a more reasonable weighted average is applied.

Implication for other IOPs or AOPs inferred from SAA-derived $a^{RS}(\lambda)$ and $b_b^{RS}(\lambda)$

For an ocean color processing system centered on IOPs, other useful properties can be further calculated from the SAA-derived $a^{RS}(\lambda)$ and $b_b^{RS}(\lambda)$. These include, for example, the $K_d(\lambda)$, the Secchi disk depth (Z_{SD}, in m), $a_{ph}(\lambda)$, and concentration of suspended particulate matter (C_{SPM}, in $g\,m^{-3}$). For stratified waters with a layer of maximum constituents deeper down from surface, as shown above, because $a^{RS}(\lambda)$ and $b_b^{RS}(\lambda)$ will tend to be lower than the weighed average, thus $K_d(\lambda)$ calculated from these $a^{RS}(\lambda)$ and $b_b^{RS}(\lambda)$ (Gordon 1989*a*; Lee et al. 2005) will also tend to be smaller than their weighted average or those derived from a linear regression between $\ln(E_d(z))$ and z (Austin and Petzold 1981; Mueller and Trees 1997). Here, $E_d(z)$ is downwelling irradiance at depth z. Such a pattern of "underestimation" will also propagate to C_{SPM} (when derived from b_{bp}^{RS}) and $a_{ph}(\lambda)$, as these properties are proportional to $a^{RS}(\lambda)$ and $b_b^{RS}(\lambda)$. On the other hand, Z_{SD} is a function of inverse K_d (Lee et al. 2015*b*), then the above-mentioned underestimation of $K_d(\lambda)$ for stratified waters will likely result in an overestimation of Z_{SD} for such cases.

Robustness of r_{rs} model for stratified waters

Based on Monte Carlo simulations, Gordon (1992) showed that r_{rs} of stratified waters can still be modeled using Eq. 4, with u a vertically weighted average. This is also confirmed with HL simulations for variation of IOPs determined by Chl alone, as shown in Fig. 5 of two Chl profiles. The averaged absolute relative difference between HL-simulated and Eq. 4 modeled r_{rs} (400–800 nm, with $<u>_Z$ for Eq. 4) is ~ 6%. Larger differences are found for wavelengths longer than 700 nm, likely due to not separating the impacts of molecular vs. particle scattering phase functions (Morel and Loisel 1998; Lee et al. 2004) when r_{rs} is modeled with a formula like Eq. 4. In these simulations, however, there is just one scattering phase function used for phytoplankton and associated detritus, and this phase function is kept the same vertically, although there are changes of Chl with the increase of depth. For stratified waters, especially at river plume regions, the particles will hardly be solely phytoplankton, rather there could be varying mixtures of phytoplankton and suspended particulate matter (Chen et al. 2018). Even if it is just phytoplankton, with the increase of Chl with depth, likely there will be changes in

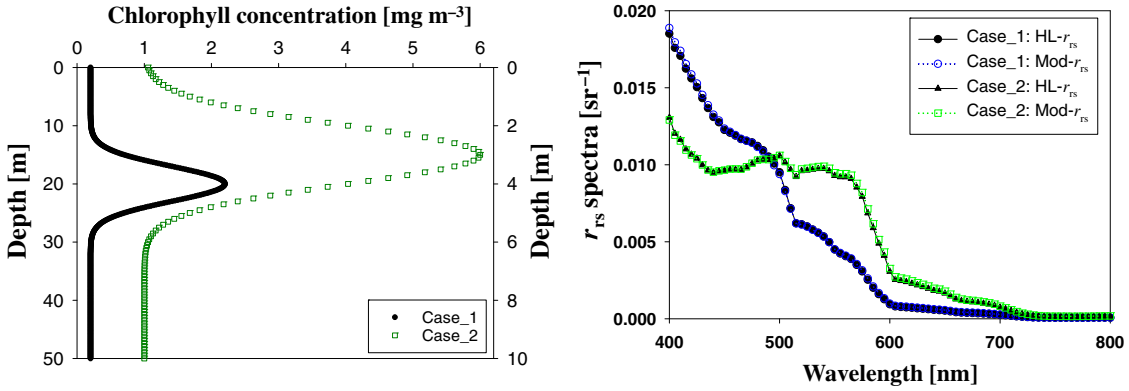

Fig. 5. (Right) Comparison between HL-simulated r_{rs} (black color) and analytical equation (Eq. 4) modeled r_{rs} (green color) for two Chl profiles (left). For Case_2 Chl profile, its Y-axis is on the right side and z_{max} = 3 m.

composition and size, thus the scattering phase function for phytoplankton will likely also change with depth (Morel and Maritorena 2001; Sullivan and Twardowski 2009). When two different scattering phase functions are associated with phytoplankton and SPM, however, differences as large as ~ 17% can be found between HL simulated and Eq. 4 modeled r_{rs} (*see* Fig. 6). In such a case, if QAA is applied, the errors associated with the r_{rs} model will be propagated to the derived b_b^{RS} and a^{RS}. For SOA type of algorithms, part of the errors in r_{rs} modeling will be propagated to the error function ($\delta_{R_{rs}}$), while at the same time it will be more challenging to properly model the spectral shape functions of a_{ph}^*, a_{dg}^*, and b_{bp}^* and then introduce errors in the derived b_b^{RS} and a^{RS}. In short, because fundamentally r_{rs} is a weighted sum of IOP contributions in the water column, it becomes an extremely complex problem to invert such an r_{rs} spectrum if there are wide ranges of particles in the water column. It will demand more detailed information of the nature of these constituents and its vertical variations to better model κ_u, r_{rs} and explain remotely sensed IOPs (Sathyendranath and Platt 1989; Forget et al. 2001; Kutser et al. 2008).

IOPs derived from a combination of R_{rs} and K_d

Remote sensing algorithms (Loisel and Stramski 2000; Loisel et al. 2018) were also developed to invert $a^{RS}(\lambda)$ and $b_b^{RS}(\lambda)$ from a combination of R_{rs} and K_d (termed as RKA hereon for such R_{rs}-K_d algorithms). This is based on that both R_{rs} and K_d are functions of a and b_b (Gordon et al. 1988; Gordon 1989*b*; Lee et al. 2013); therefore, it is a system of two equations for two unknowns. When $a^{RS}(\lambda)$ and $b_b^{RS}(\lambda)$ are inverted from $R_{rs}(\lambda)$ via RKA, however, $K_d(\lambda)$ is first estimated from the $R_{rs}(\lambda)$ spectrum through empirical regressions (Loisel et al. 2001) or neural networks (Loisel et al. 2018), that is, the $K_d(\lambda)$ in RKA is not an independent measurement. Because generally a dominates K_d at a given wavelength for most natural waters (Gordon 1989*b*; Lee et al. 2013), $a^{RS}(\lambda)$ inverted via RKA is

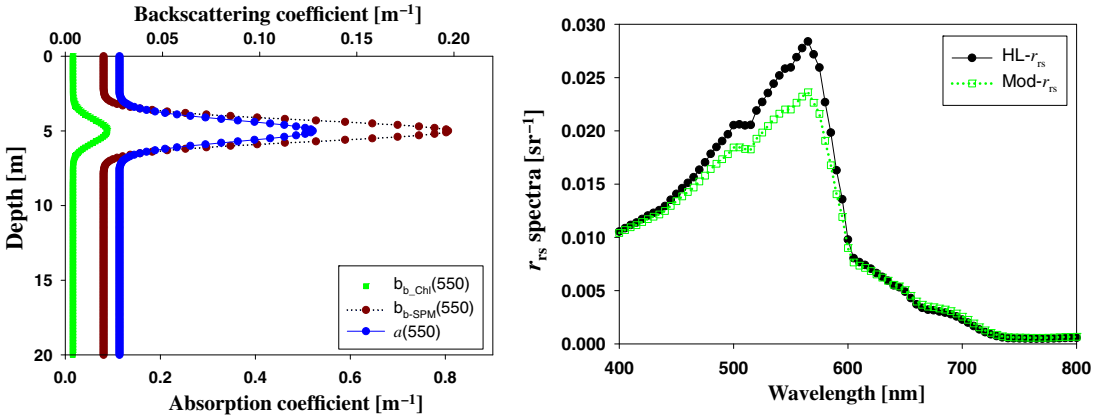

Fig. 6. As Fig. 5, (Right) a comparison between HL-simulated r_{rs} (black color) and analytical equation (Eq. 4) modeled r_{rs} (green color) for a synthetic water column having both phytoplankton and SPM (both have maximum values at 5 m), with the profiles of a(550), b_{b_ph}(550), and b_{b_SPM}(550) showing in the left side. The scattering phase function for phytoplankton is a Fournier-Forand phase function (Fournier and Forand 1994) with a backscattering ratio of 1%, while it is Petzold-averaged phase function (Petzold 1972; Mobley 1994) for SPM (backscattering ratio is 1.8%).

mainly dependent on the empirically estimated $K_d^{RS}(\lambda)$, with $b_b^{RS}(\lambda)$ mainly determined from $R_{rs}(\lambda)$ and the inverted $a^{RS}(\lambda)$. As such, the picture of the inverted $a^{RS}(\lambda)$ and $b_b^{RS}(\lambda)$ via RKA is not clear when the water is stratified. This is because if the algorithm for $K_d^{RS}(\lambda)$ was developed for vertically homogeneous waters (Loisel et al. 2001; Jamet et al. 2012), when an R_{rs} spectrum of stratified waters is the input, similarly like the empirically estimated Chl from R_{rs}, the resulted $K_d^{RS}(\lambda)$ from $R_{rs}(\lambda)$ of stratified waters could be significantly lower or higher than its weighted average (if also calculated following Eq. 2) (Gordon 1992; Stramska and Stramski 2005). Subsequently this uncertainty will be propagated to the calculated $a^{RS}(\lambda)$ and $b_b^{RS}(\lambda)$ via the RKA. An algorithm for $K_d(\lambda)$ of stratified waters is required for application of RKA to such waters, which will then be highly dependent on the data characteristics used to train the empirical algorithm.

Chl^{RS} from empirical algorithms

Presently the generation of chlorophyll concentration (Chl^{RS}) from satellite ocean color commonly takes an empirical approach with ratios of R_{rs} as the input (*see* Eq. 1 for an example), and there have been quite many sensitivity studies (Sathyendranath and Platt 1989; Stramska and Stramski 2005; Kutser et al. 2008) to highlight the impact of stratified waters on the empirical retrieval of Chl when algorithms developed for homogeneous waters are used. However, we need to keep in mind that the algorithm coefficients (e.g., values of α_{0-4} in Eq. 1) are driven by the data pooled together for the development of such algorithms, which is a nature of all empirical algorithms (O'Reilly et al. 1998; Werdell and Bailey 2005; Hu et al. 2012; Shang et al. 2019). For the operational Chl algorithm adopted by NASA OBPG, the required Chl and R_{rs} were pooled from global contributions with ~ 4000 colocated Chl and multispectral R_{rs}. For such a large data set, roughly 50% have vertical profiles of Chl (Werdell and Bailey 2005; J. Werdell pers. comm.), while the other half have only subsurface Chl (represented as Chl_{SS} hereon). For the ~ 50% data with vertical Chl profiles, a weighted average for each profile was calculated following Eq. 2 using the weighting profile calculated at 490 nm (represented as <Chl(490)> hereon). Therefore, the chlorophyll concentrations used for the algorithm development were a mixture of Chl_{SS} and <Chl(490)>, each about 50%. With such a data set, the target of the empirical algorithm is ambiguous. This is because:

1. Chl_{SS} and <Chl(490)> are not the same type of property and can differ a lot. For example, $<Chl(490)>_Z$ is ~ 74% higher than Chl at 1 m for the case showing in Fig. 1.
2. Weighting profile is wavelength-dependent. $<Chl(490)>_Z$ is not necessarily matching the weighted chlorophyll concentration at 440 or 510 nm, or that from an R_{rs} ratio. Using the case showing in Fig. 1 as an example, $<Chl(490)>_Z$ is ~ 26% higher than $<Chl(510)>_Z$ and ~ 36% higher than $<Chl(530)>_Z$, where such ratios vary with profiles.
3. Although ~ 50% of the data set have <Chl(490)>, to what extent these Chl(z) were stratified are not clear. One possible scenario could be that the waters of Chl_{SS} were more stratified than the waters of <Chl(490)>.

Because the Chl data used for the algorithm development is a mixture, more uncertainties could be introduced in the empirically estimated Chl^{RS}. In addition, it is necessary to keep in mind that, as Gordon (1992) and Zaneveld et al. (2005) pointed out, the match between band-ratio Chl and $<Chl(\lambda)>_G$ (or $<Chl(\lambda)>_Z$) will deteriorate if the profiles of absorption and backscattering coefficients do not covary, but such information about IOPs profiles was not available or not considered during the phase of the algorithm development.

Since it is R_{rs} representing the weighted average of the upper water column and OC4 algorithm (or any other empirical algorithms) is empirical in nature, it could be better and easier to simply pool Chl_{SS} for the development of empirical algorithms, regardless if the water column is stratified or not. With such a data set, the resulted α_{0-4} will to some degree compensate subsurface stratification information when Eq. 1 is forced to match Chl_{SS}, if the data include stratified waters. Furthermore, there will be no ambiguity regarding the resulted Chl^{RS} from such an algorithm, which then reduces uncertainties when Chl^{RS} is compared with in situ measurements. For a Chl^{RS} product comparable with that of Eq. 2, values of $<Chl(\lambda)>_G$ (or $<Chl(\lambda)>_Z$) must be employed during the development or tuning of the empirical algorithms. In particular, the wavelength(s) and the method of weighting must be clearly spelled out (Werdell and Bailey 2005), and must be followed exactly when later measurements are used to validate remote sensing products from such algorithms, otherwise it will be an apple-vs.-orange comparison. Recently Valente et al. (2016) developed a large bio-optical dataset for ocean color applications, where the Chl data are simple average of measured Chl of the upper 10 m under the condition that the coefficient of variation among the measurements is less than 50%. Such a data set excluded strongly stratified waters if the stratification happened within top 10 m, but may include data such as those showing in Fig. 1. It appears that for stratified waters, a detailed comparison of using subsurface value vs. using different averages is necessary for a complete understanding of the pros and cons for the development of empirical algorithms or for the validation of algorithm retrievals.

Conclusions

Through theoretical derivations, Zaneveld et al. (2005) showed that for stratified waters, r_{rs} can be considered as a function of weighted average of $b_b(z)/(a(z) + b_b(z))$ by assuming no vertical variation of the modeling coefficients, with

the weighting factor a combination of the round-trip exponential attenuation of light as well as the vertical profile of the attenuation ($\tau(z)$). Based on this model and the analytical nature of QAA, it is found that the resulted IOPs and Chl retrieved via QAA (or SAA) cannot be evaluated using the classic model of weighted average. Rather, they are associated with complex relationships with their vertical distributions. In general:

1. The inverted b_b (and then b_{bp}) has limited b_b information from deeper depths due to the use of longer wavelengths in the inversion process. Because of this nature, for cases with a subsurface maximum chlorophyll, the $b_b^{RS}(\lambda)$ product in the shorter (more transparent) wavelengths will tend to be lower compared to the vertically weighted average with weighting factors calculated at the wavelength of interest; and, the spectral variation of the b_b^{RS} spectrum will not be able to capture the spectral feature of the vertically weighted average b_b spectrum. It is more appropriate to use b_b weighted using weighting factors of the longer wavelengths to evaluate b_b^{RS} obtained with SAA algorithms.
2. The inverted absorption coefficient is weighted by the weighting factor of b_b in the longer wavelength(s), as well as the weighting factor in the wavelength of interest. As a result, the inverted absorption coefficient in the shorter (more transparent) wavelengths will tend to be lower than the vertically weighted average (assuming perfect QAA or SAA developed for homogeneous waters), unless the surface layer dominates the diffuse attenuation of light. Or, to properly evaluate the absorption coefficient obtained with SAA algorithms, the weighted average should be modulated by backscattering coefficient following Eq. 23.
   In addition, for application of QAA to both homogeneous and stratified waters, the estimation of the absorption coefficient at the reference wavelength should be tuned using vertically weighted averages.
3. Furthermore, because SAA-inverted Chl is mainly inferred from the absorption coefficient, the Chl product (assuming perfect bio-optical relationships) will also tend to be lower than the vertically weighted average if the layer of maximum chlorophyll is not at sea surface.
4. The picture becomes much more complex for situations where particle types and/or sizes differ with the increase of depth, which will result in a change of particle phase functions and then errors in r_{rs} calculation if the current model is applied, because the current r_{rs} model was developed based on a vertically constant (and same) scattering phase function for all particulates. Therefore, for stratified waters, the uncertainties will not simply arise from the vertical distribution of chlorophyll concentration, also from the nature of all constituents in the vertical dimension.

On the other hand, for empirical Chl algorithms, because of the use of mixed Chl at the development phase of present empirical algorithms, Chl^{RS} estimated from the present OC4-type empirical algorithms is not necessarily a representation of the vertically weighted average Chl at 490 nm. To avoid ambiguity about this data product, it might be better, at the development phase of such empirical algorithms, to pool subsurface Chl value and let the algorithm coefficients to compensate any effects due to water column stratification. This is also because that the weighted average scheme could run into large uncertainties if the profiles of scattering and absorption coefficients do not covary.

The above describes the overall nature of the remote sensing products of stratified waters when they are derived from a remote sensing reflectance spectrum, as well as a theoretical framework to subsequently pursue detailed analysis of the products retrieved via an SAA for stratified waters. The characteristics of remote sensing products are important to reduce uncertainties in evaluation of IOPs and Chl products of stratified waters when they are compared with field measurements. It also emphasizes the importance to obtain detailed information of water constituents in the vertical dimension, because fundamentally it is r_{rs} (R_{rs}) a weighted average of the upper water column, while remote sensing products are algorithm-dependent, especially the weighting factor varies spectrally.

References

Aas, E. 1987. Two-stream irradiance model for deep waters. Appl. Opt. **26**: 2095–2101. doi:10.1364/AO.26.002095.

Antoine, D., and others. 2011. Variability in optical particle backscattering in contrasting bio-optical oceanic regimes. Limnol. Oceanogr. **56**: 955–973. doi:10.4319/lo.2011.56.3.0955.

Austin, R. W., and T. J. Petzold. 1981. The determination of the diffuse attenuation coefficient of sea water using the coastal zone color scanner, p. 239–256. *In* J. F. R. Gower [ed.], Oceanography from space. Plenum Press.

Boyce, D. G., M. Dowd, M. R. Lewis, and B. Worm. 2014. Estimating global chlorophyll changes over the past century. Prog. Oceanogr. **122**: 163–173. doi:10.1016/j.pocean.2014.01.004.

Bricaud, A., M. Babin, A. Morel, and H. Claustre. 1995. Variability in the chlorophyll-specific absorption coefficients of natural phytoplankton: Analysis and parameterization. J. Geophys. Res. **100**: 13321–13332. doi:10.1029/95JC00463.

Chen, S., and T. Zhang. 2015. Evaluation of a QAA-based algorithm using MODIS land bands data for retrieval of IOPs in the Eastern China Seas. Opt. Express **23**: 13953–13971. doi:10.1364/OE.1323.013953.

Chen, S., T. Zhang, L. Hu, C. Xue, and X. Wu. 2018. Vertical variations in optical properties of the waters in the Yellow Sea and Bohai Sea at seasonal scales and their influencing mechanisms. Opt. Express **26**: 4112–4134. doi:10.1364/OE.1326.004112.

Churnside, J. H., and P. L. Donaghay. 2009. Thin scattering layers observed by airborne lidar. ICES J. Mar. Sci. **66**: 778–789. doi:10.1093/icesjms/fsp1029.

Cullen, J. J. 2015. Subsurface chlorophyll maximum layers: Enduring enigma or mystery solved? Ann. Rev. Mar. Sci. **7**: 207–239. doi:10.1146/annurev-marine-010213-135111.

Defoin-Platel, M., and M. Chami. 2007. How ambiguous is the inverse problem of ocean color in coastal waters? J. Geophys. Res. **112**: C03004. doi:10.01029/02006JC003847.

Doerffer, R., and J. Fisher. 1994. Concentrations of chlorophyll, suspended matter, and gelbstoff in case II waters derived from satellite coastal zone color scanner data with inverse modeling methods. J. Geophys. Res. **99**: 7457–7466. doi:10.1029/93JC02523.

Dong, Q., S. Shang, and Z. Lee. 2013. An algorithm to retrieve absorption coefficient of chromophoric dissolved organic matter from ocean color. Remote Sens. Environ. **128**: 259–267. doi:10.1016/j.rse.2012.10.013.

Forget, P., P. Broche, and J.-J. Naudin. 2001. Reflectance sensitivity to solid suspended sediment stratification in coastal water and inversion: A case study. Remote Sens. Environ. **77**: 92–103.

Fournier, G. R., and J. L. Forand. 1994. Analytic phase function for ocean water, p. 194–201. *In* J. Jaffe [ed.], Ocean optics XII. SPIE.

Gomes, A., N. Bernardo, A. Carmo, T. Rodrigues, and E. Alcântara. 2018. Diffuse attenuation coefficient retrieval in CDOM dominated inland water with high chlorophyll-a concentrations. Remote Sens. **10**: 1063. doi:10.3390/rs10071063.

Gordon, H. R. 1989*a*. Can the Lambert-Beer law be applied to the diffuse attenuation coefficient of ocean water? Limnol. Oceanogr. **34**: 1389–1409.

Gordon, H. R. 1989*b*. Dependence of the diffuse reflectance of natural waters on the sun angle. Limnol. Oceanogr. **34**: 1484–1489.

Gordon, H. R. 1992. Diffuse reflectance of the ocean: Influence of nonuniform phytoplankton pigment profile. Appl. Opt. **31**: 2116–2129. doi:10.1364/AO.31.002116.

Gordon, H. R., and W. R. Mcluney. 1975. Estimation of the depth of sunlight penetration in the sea for remote sensing. Appl. Opt. **14**: 413–416. doi:10.1364/AO.14.000413.

Gordon, H. R., and D. K. Clark. 1980. Remote sensing optical properties of a stratified ocean: An improved interpretation. Appl. Opt. **19**: 3428–3430. doi:10.1364/AO.19.003428.

Gordon, H. R., D. K. Clark, J. W. Brown, O. B. Brown, R. H. Evans, and W. W. Broenkow. 1983. Phytoplankton pigment concentrations in the Middle Atlantic Bight: Comparison of ship determinations and CZCS estimates. Appl. Opt. **22**: 20–36. doi:10.1364/AO.22.000020.

Gordon, H. R., and A. Morel. 1983. Remote assessment of ocean color for interpretation of satellite visible imagery: A review. Springer-Verlag.

Gordon, H. R., and others. 1988. A semianalytic radiance model of ocean color. J. Geophys. Res. **93**: 10909–10924.

Gregg, W. W., and M. E. Conkright. 2002. Decadal changes in global ocean chlorophyll. Geophys. Res. Lett. **29**: 1730. doi:10.1029/2002GL014689.

Grunert, B. K., C. B. Mouw, and A. B. Ciochetto. 2019. Deriving inherent optical properties from decomposition of hyperspectral non-water absorption. Remote Sens. Environ. **225**: 193–206. doi:10.1016/j.rse.2019.03.004.

Hu, C., Z. Lee, and B. Franz. 2012. Chlorophyll a algorithms for oligotrophic oceans: A novel approach based on three-band reflectance difference. J. Geophys. Res. **117**: C01011. doi:10.01029/02011JC007395.

Huang, S., Y. Li, S. Shang, and S. Shang. 2013. Impact of computational methods and spectral models on the retrieval of optical properties via spectral optimization. Opt. Express **21**: 6257–6273. doi:10.1364/OE.21.006257.

IOCCG. 2000. Remote sensing of ocean colour in coastal, and other optically-complex, waters. *In* S. Sathyendranath [ed.], Reports of the International Ocean-Colour Coordinating Group, No.3. IOCCG. 140.

IOCCG. 2006. Remote sensing of inherent optical properties: Fundamentals, tests of algorithms, and applications, p. 126. *In* Z. P. Lee [ed.], Reports of the International Ocean-Colour Coordinating Group, No. 5. IOCCG.

Jamet, C., H. Loisel, and D. Dessailly. 2012. Retrieval of the spectral diffuse attenuation coefficient $K_d(\lambda)$ in open and coastal ocean waters using a neural network inversion. J. Geophys. Res. **117**: C10023. doi:10.11029/12012JC008076.

Kutser, T., L. Metsamaa, and A. G. Dekker. 2008. Influence of the vertical distribution of cyanobacteria in the water column on the remote sensing signal. Estuar. Coast. Shelf Sci. **78**: 649–654. doi:10.1016/j.ecss.2008.02.024.

Lee, Z. P., K. L. Carder, C. D. Mobley, R. G. Steward, and J. S. Patch. 1999. Hyperspectral remote sensing for shallow waters: 2. Deriving bottom depths and water properties by optimization. Appl. Opt. **38**: 3831–3843. doi:10.1364/AO.38.003831.

Lee, Z. P., K. L. Carder, and R. Arnone. 2002. Deriving inherent optical properties from water color: A multi-band quasi-analytical algorithm for optically deep waters. Appl. Opt. **41**: 5755–5772. doi:10.1364/AO.41.005755.

Lee, Z. P., K. L. Carder, and K. P. Du. 2004. Effects of molecular and particle scatterings on model parameters for remote-sensing reflectance. Appl. Opt. **43**: 4957–4964. doi:10.1364/AO.43.004957.

Lee, Z. P., M. Darecki, K. L. Carder, C. O. Davis, D. Stramski, and W. J. Rhea. 2005. Diffuse attenuation coefficient of downwelling irradiance: An evaluation of remote sensing methods. J. Geophys. Res. Oceans **110**: C02017.

Lee, Z. P., R. Arnone, C. Hu, P. J. Werdell, and B. Lubac. 2010. Uncertainties of optical parameters and their propagations in an analytical ocean color inversion algorithm. Appl. Opt. **49**: 369–381. doi:10.1364/AO.49.000369.

Lee, Z. P., and others. 2013. Penetration of UV-visible solar light in the global oceans: Insights from ocean color remote sensing. J. Geophys. Res. **118**: 4241–4255. doi:10.1002/jgrc.20308.

Lee, Z. P., J. Wei, K. Voss, M. Lewis, A. Bricaud, and Y. Huot. 2015*a*. Hyperspectral absorption coefficient of "pure" seawater in the range of 350–550 nm inverted from remote sensing reflectance. Appl. Opt. **54**: 546–558. doi:10.1364/AO.54.000546.

Lee, Z. P., and others. 2015*b*. Secchi disk depth: A new theory and mechanistic model for underwater visibility. Remote Sens. Environ. **169**: 139–149.

Loisel, H., and A. Morel. 1998. Light scattering and chlorophyll concentration in case 1 waters: A reexamination. Limnol. Oceanogr. **43**: 847–858. doi:10.4319/lo.1998.43.5.0847.

Loisel, H., and D. Stramski. 2000. Estimation of the inherent optical properties of natural waters from the irradiance attenuation coefficient and reflectance in the presence of Raman scattering. Appl. Opt. **39**: 3001–3011. doi:10.1364/AO.39.003001.

Loisel, H., and others. 2001. Comparison of the ocean inherent optical properties obtained from measurements and inverse modeling. Appl. Opt. **40**: 2384–2397. doi:10.1364/AO.40.002384.

Loisel, H., D. Stramski, D. Dessailly, C. Jamet, L. Li, and R. A. Reynolds. 2018. An inverse model for estimating the optical absorption and backscattering coefficients of seawater from remote-sensing reflectance over a broad range of oceanic and coastal marine environments. J. Geophys. Res. Oceans **123**: 2141–2171. doi:10.1002/2017JC013632.

Maritorena, S., D. A. Siegel, and A. R. Peterson. 2002. Optimization of a semianalytical ocean color model for global-scale applications. Appl. Opt. **41**: 2705–2714. doi:10.1364/AO.41.002705.

Mobley, C. D. 1994. Light and water: Radiative transfer in natural waters. Academic Press.

Mobley, C. D., and L. K. Sundman. 2013. HydroLight 5.2 user's guide. Sequoia Scientific.

Moore, T. S., and others. 2019. Vertical distributions of blooming cyanobacteria populations in a freshwater lake from LIDAR observations. Remote Sens. Environ. **225**: 347–367.

Morel, A., and J. F. Berthon. 1989. Surface pigments, algal biomass profiles, and potential production of the euphotic layer: Relationships reinvestigated in review of remote-sensing applications. Limnol. Oceanogr. **34**: 1545–1562. doi:10.4319/lo.1989.34.8.1545.

Morel, A., and H. Loisel. 1998. Apparent optical properties of oceanic water: Dependence on the molecular scattering contribution. Appl. Opt. **37**: 4765–4776. doi:10.1364/AO.37.004765.

Morel, A., and S. Maritorena. 2001. Bio-optical properties of oceanic waters: A reappraisal. J. Geophys. Res. **106**: 7163–7180. doi:10.1029/2000JC000319.

Mueller, J. L., and C. C. Trees [eds.]. 1997. Revised sea WIFS prelaunch algorithm for diffuse attenuation coefficient K (490). NASA Goddard Space Flight Center.

O'Reilly, J., and others. 1998. Ocean color chlorophyll algorithms for SeaWiFS. J. Geophys. Res. **103**: 24937–24953. doi:10.1029/98JC02160.

Park, Y. J., and K. Ruddick. 2005. Model of remote-sensing reflectance including bidirectional effects for case 1 and case 2 waters. Appl. Opt. **44**: 1236–1249. doi:10.1364/AO.44.001236.

Petzold, T. J. 1972. Volume scattering functions for selected natural waters, p. 72–78. Scripps Institute of Oceanography.

Philpot, W. D. 1987. Radiative transfer in stratified waters: A single-scattering approximation for irradiance. Appl. Opt. **26**: 4123–4132. doi:10.1364/AO.26.004123.

Platt, T., S. Sathyendranath, C. M. Caverhill, and M. Lewis. 1988. Ocean primary production and available light: Further algorithms for remote sensing. Deep-Sea Res. Part A Oceanogr. Res. Pap. **35**: 855–879.

Pope, R., and E. Fry. 1997. Absorption spectrum (380 - 700 nm) of pure waters: II. Integrating cavity measurements. Appl. Opt. **36**: 8710–8723. doi:10.1364/AO.36.008710.

Preisendorfer, R. W. 1976. Hydrologic optics. Introduction, v. 1. Also available on CD. National Technical Information Service, Office of Naval Research.

Roesler, C. S., and M. J. Perry. 1995. In situ phytoplankton absorption, fluorescence emission, and particulate backscattering spectra determined from reflectance. J. Geophys. Res. **100**: 13279–13294. doi:10.1029/95JC00455.

Sathyendranath, S., and T. Platt. 1989. Remote sensing of ocean chlorophyll: Consequence of nonuniform pigment profile. Appl. Opt. **28**: 490–495. doi:10.1364/AO.28.000490.

Shang, S., Z. P. Lee, G. Lin, Y. Li, and X. Li. 2019. Progressive scheme for blending empirical ocean color retrievals of absorption coefficient and chlorophyll concentration from open oceans to highly turbid waters. Appl. Opt. **58**: 3360–3369.

Signorini, S. R., B. A. Franz, and C. R. McClain. 2015. Chlorophyll variability in the oligotrophic gyres: Mechanisms, seasonality and trends. Front. Mar. Sci. **2**: 1–11. doi:10.3389/fmars.2015.00001.

Smith, R. C. 1981. Remote sensing and depth distribution of ocean chlorophyll. Mar. Ecol. Prog. Ser. **5**: 359–361.

Stramska, M., and D. Stramski. 2005. Effects of a nonuniform vertical profile of chlorophyll concentration on remote-sensing reflectance of the ocean. Appl. Opt. **44**: 1735–1747. doi:10.1364/AO.44.001735.

Sullivan, J. M., and M. S. Twardowski. 2009. Angular shape of the oceanic particulate volume scattering function in the backward direction. Appl. Opt. **48**: 6811–6819. doi:10.1364/AO.48.006811.

Twardowski, M., and A. Tonizzo. 2018. Ocean color analytical model explicitly dependent on the volume scattering function. Appl. Sci. **8**: 2684. doi:10.3390/app8122684.

Valente, A., and others. 2016. A compilation of global bio-optical in situ data for ocean-colour satellite applications. Earth Syst. Sci. Data **8**: 235–252.

Werdell, P. J., and S. W. Bailey. 2005. An improved bio-optical data set for ocean color algorithm development and satellite data product validation. Remote Sens. Environ. **98**: 122–140. doi:10.1016/j.rse.2005.07.001.

Werdell, P. J., B. A. Franz, J. T. Lefler, W. D. Robinson, and E. Boss. 2013*a*. Retrieving marine inherent optical properties from satellites using temperature and salinitydependent backscattering by seawater. Opt. Express **21**: 32611–32622. doi:10.1364/OE.21.032611.

Werdell, P. J., and others. 2013*b*. Generalized ocean color inversion model for retrieving marine inherent optical properties. Appl. Opt. **52**: 2019–2037.

Werdell, P. J., C. S. Roesler, and J. I. Goes. 2014. Discrimination of phytoplankton functional groups using an ocean reflectance inversion model. Appl. Opt. **53**: 4833–4849. doi:10.1364/AO.53.004833.

Werdell, P. J., and others. 2018. An overview of approaches and challenges for retrieving marine inherent optical properties from ocean color remote sensing. Prog. Oceanogr. **160**: 186–212. doi:10.1016/j.pocean.2018.01.001.

Xue, K., Y. Zhang, H. Duan, R. Ma, S. Loiselle, and M. Zhang. 2015. A remote sensing approach to estimate vertical profile classes of phytoplankton in a eutrophic lake. Remote Sens. **7**: 14403–14427. doi:10.3390/rs71114403.

Zaneveld, J. R. V., A. H. Barnard, W. S. Pegau, and E. Boss. 1998. An investigation into the appropriate depth average of remotely sensed optical parameters. *In* S. Ackleson and J. Campbell [eds.], Ocean optics XIV. SPIE.

Zaneveld, J. R. V., A. H. Barnard, and E. Boss. 2005. Theoretical derivation of the depth average of remotely sensed optical parameters. Opt. Express **13**: 9052–9061. doi:10.1364/OPEX.13.009052.

Zhang, X., L. Hu, and M.-X. He. 2009. Scattering by pure seawater: Effect of salinity. Opt. Express **17**: 5698–5710. doi:10.1364/OE.17.005698.

Zheng, G., D. Stramski, and P. M. DiGiacomo. 2015. A model for partitioning the light absorption coefficient of natural waters into phytoplankton, nonalgal particulate, and colored dissolved organic components: A case study for the Chesapeake Bay. J. Geophys. Res. Oceans **120**: 2601–2621. doi:10.1002/2014JC010604.

Acknowledgments

We thank the two anonymous reviewers for constructive comments and suggestions that greatly improved this manuscript. Financial support from the Chinese Ministry of Science and Technology (2016YFC1400905 and 2016YFA0601201 to Shang), the National Natural Science Foundation of China (41830102 and 41776184, to Shang; http://www.nsfc.gov.cn/english/site_1/index.html), the National Oceanic and Atmospheric Administration (NOAA) JPSS VIIRS Ocean Color Cal/Val Project (NA11OAR4320199 to Lee), and the University of Massachusetts Boston is greatly appreciated.

Conflict of Interest

None declared.

Submitted 25 February 2019
Revised 03 June 2019
Accepted 23 July 2019

Associate editor: David Antoine